Chemical Vapor Infiltration: Dispersed and Graded Depositions for Ceramic Composites

G. Y. Chung, B. J. McCoy, and J. M. Smith
Dept. of Chemical Engineering, University of California, Davis, CA 95616

Domenick E. Cagliostro
NASA Ames Research Center, Moffett Field, CA 94035

A structured-geometry model for dispersed and graded deposits was developed for chemical vapor infiltration of multiply-woven substrates of carbon filters. An earlier model was modified to allow for two reactants in the feed. The model predicts gas-phase concentration profiles in the voids of substrates and deposition amounts of two reactants as a function of time and location. Results are shown for feeding reactant gases simultaneously for dispersed deposition and periodically for the study of the graded deposition for a typical substrate. The variation in relative contents of reactants in the feed with time shows how the composition of the deposit varies. Porosities and changes of dimensions with time everywhere in the substrate are also predicted. This is an advantage of the structured-geometry model vs. a simplified homogeneous geometry for the substrate. Such a simplification may preclude predicting failure, such as delamination, which would require a local description of the composite structure.

Sensitivity to input parameters such as temperature, pressure, and reactant feed concentration is discussed, and two substrate geometries are compared.

The behavior of the system is predicted to be dominated by the times to fill gaps between filaments at the ply surfaces and the outermost space between plies. Furthermore, faster kinetics and slower reactant diffusion favor deposition of one material near the surface of a ply or the matrix and the other near the center of the ply or matrix. By manipulating feed rates of reactants, uniformity of material and overall porosity of the composites are predicted to be enhanced.

Introduction

Ceramic materials have good mechanical properties at high temperatures, low density, and resistance to corrosion and erosion. Fiber reinforcement adds strength and toughness. Such fiber-reinforced composites can be prepared, for example, by sintering and hotpressing of mixtures of powders and chopped fibers and by chemical vapor infiltration (CVI). One advantage of CVI is that the fibers are not stressed during preparation.

During deposition, reactant gases diffuse from the outside surface of the sample, introducing an internal concentration gradient. This gradient can result in a deposition profile in the composite and occlusion of the outer surface of the sample before filling all the interior voids. Periodic pressurization and depressurization or applying a temperature gradient across the substrate have been proposed to compensate for the effects of decreasing concentration of reactant gases.

Mathematical models of the deposition process have also been developed to understand the relationship between the chemical reaction rate and various mass transport mechanisms. These models include those for deposition in a cylindrical tube or pore (van den Brekel et al., 1981; Gupte and Tsamopoulos, 1989) and on short fiber preforms based on a unit cell of intersecting cylinders (Starr, 1987). The Gupte and Tsamo-

Correspondence concerning this article should be addressed to J. M. Smith.

Table 1. Parameter Values Used to Illustrate the Model for Different Feed Procedures

Initial Dimensions of the Sample			
	$a_o = 0.06$ cm	$b_o = 0.003$ cm	
	$c_o = 0.024$ cm	$d_o = 0.18$ cm	
	$r_o = 0.0004$ cm	$H = 0.348$ cm	
	$N = 13$,	$W = 695{,}000$ cm^{-2}	
	No. of filaments in a tow = 3,000		
Deposition Conditions			
	Pressure	10 torr	
	Temperature	925°C	
D_{mS}	17,900 cm^2/min	D_{mT}	6,700 cm^2/min
k_S	10.0 cm/min	k_T	35.0 cm/min
ρ_{mS}	3.2 g/cm^3	ρ_{mT}	4.5 g/cm^3
C_{So} (2.4% DDS)	3.21×10^{-9} mol/cm^3	C_{To} (1.0% $TiCl_4$)	1.34×10^{-9} mol/cm^3

	DDS	$TiCl_4$	
Cases I and 3:	2.4%	1.0%	codeposition
Case II: 0–5 h	1.5%	2.0%	graded deposition
5–10 h	2.0%	1.5%	
after 10 h	2.4%	1.0%	

poulos model is based on a Bethe lattice and on porous solids by Jensen and Melkote (1989) and Sotirchos and Tomadakis (1989). Also models have been proposed for a fiber bundle based on cylindrical pores (Rossignol et al., 1984; Tai and Chou, 1989) and based on a random overlap model (Currier, 1990). These prior models all refer to *homogeneous* geometry within the sample. In contrast, the models of Chung et al. (1991, 1992) for layered plies of woven tows (rectangular bundles of filaments) consider the detailed distribution of void spaces and surfaces within the sample.

The Chung et al. models were for aligned holes (Chung et al., 1991) and maximum staggering (Chung et al., 1992) of the holes through the plies. These models considered diffusion in the voids and deposition on the surfaces in the holes between tows, spaces between plies, and gaps around filaments. The aligned-hole and maximum staggered-hole arrangements represent bounds of weave configuration. The staggered-hole model (maximum staggering) is applied in this research to predict intraparticle deposition and porosities for dispersed and graded deposits, that is, where two components are deposited in the weave. The two components used here are TiB_2 and SiC. Silicon carbide is produced by the chemical vapor deposition (CVD) from dichloro-dimethylsilane (DDS) and hydrogen. The model assumes that the overall deposition kinetics are first-order in DDS. Titanium diboride is also a refractory material and relatively inert to oxidation and chemical attack. Kinetic data on the CVD of TiB_2 were reported by Peshev and Niemyski (1965). Deposition rates and efficiencies for CVD of TiB_2 from $TiCl_4$, BCl_3, and H_2 were experimentally determined as a function of various variables by Besman and Spear (1977). They fitted experimental data with the assumption that the chemical kinetic step is first-order with respect to the partial pressure of the limiting species. The same assumption that the overall deposition kinetics are first-order in $TiCl_4$, the limiting reactant, is used in this research.

The model predicts how the gaseous concentration profiles, the overall rate of deposition, the final porosity, and the dimensions in the sample change with time due to depositions of two components. The first objective was to show how the contents of each component in the deposit can be controlled by changing the relative contents of reactants in the feed. For this we tested three cases for a typical substrate: I. mixtures of constant composition of DDS and $TiCl_4$ (along with BCl_3 and H_2) enter the sample simultaneously and at constant composition throughout the whole reaction time; II. DDS and $TiCl_4$ enter simultaneously, but the compositions are programmed to change with time (see Table 1); and III. pure DDS and $TiCl_4$ enter sequentially at two-hour time intervals. Cases I and III may be described as dispersed deposition, and case II as graded deposition. As a second objective, sensitivity computations were made to show the effects of pressure, temperature, and reactant feed concentrations for two substrates of different geometry.

Model Development

The model for infiltration of SiC and TiB_2 is based on the same geometry as used for the staggered-hole model (Chung et al., 1992). Mass transfer of the reactant gases is considered to occur only by diffusion. The substrate geometry consists of 13 layers (plies) of woven fabric, as shown in Figure 1. In the plies each tow is rectangular in cross-section and consists of a bundle of nonporous filaments woven to form approximately square holes. The plies are spaced so that the holes in one ply are positioned at the center of the adjacent four holes in the upper and lower plies (maximum staggering of holes). The filaments within a tow are arranged on triangular centers. Diffusion of gaseous DDS and $TiCl_4$ occurs from both ends toward the center of the sample by going through the holes, through the spaces between plies, and through the gaps around the filaments. Because of symmetry, the model needs to consider only half of the sample. Numbering of holes, spaces and plies begins from the outside hole, space, and ply, as indicated in Figure 2.

While deposition occurs in the gaps around filaments in the inner plies, there is also deposition on the outside flat surfaces of the outer plies. Since the distance (b) between plies is small, the first space in Figure 2 is plugged before gaps around the

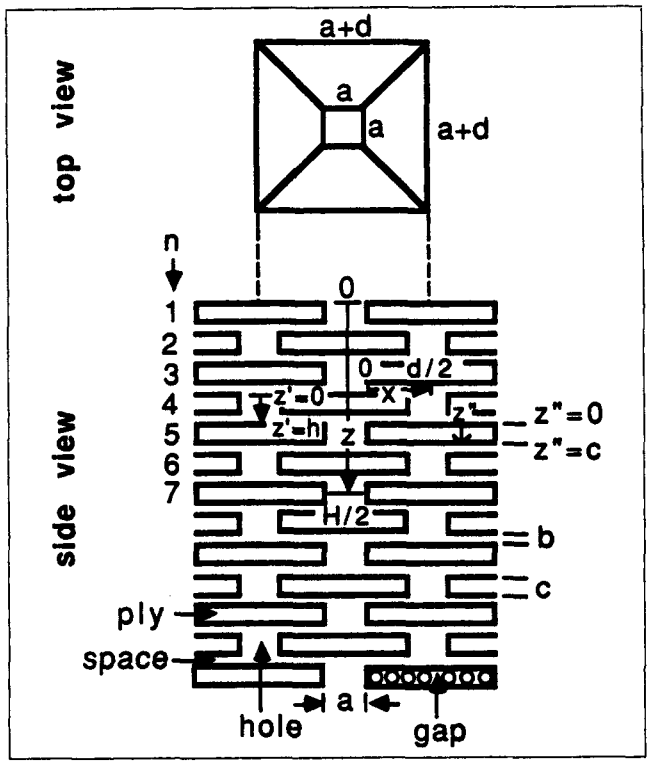

Figure 1. Notation for dimensions, number of plies, and coordinates.

The system is symmetric on either side of the 7th ply: $z = H/2$ is a plane of symmetry.

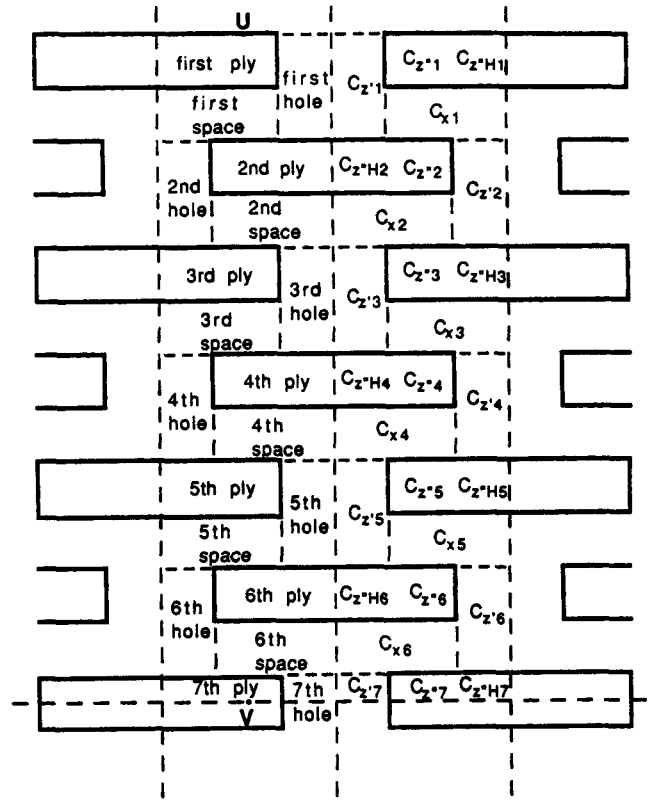

Figure 2. Notation for the concentrations in the holes ($C_{z',n}$), in the spaces between plies ($C_{x,n}$), and in the gaps around filaments ($C_{z'',n}$ & $C_{z'',H,n}$).

outer filaments of the inner plies are plugged. For this situation, deposition in the middle of the sample ceases before the gaps are filled around the outer filaments of the inner plies.

As in the staggered-hole model, the following assumptions are involved. The sample is isothermal. Diffusion is one-dimensional in the holes and the gaps around filaments, and two-dimensional in the spaces between plies. Hence, there is no concentration gradient in the x and y directions in the holes, and no concentration gradient in the z direction in the spaces between plies. The assumption that the diffusion velocity in the void regions is large with respect to the rate of change of the thickness of the deposit (Bischoff, 1963) is also used. With this assumption, gaseous diffusion in the voids can be treated as a (pseudo) steady-state process. As deposition occurs, the concentration profiles in the void regions change as the porosity and surface area change. In addition, it is assumed that there is negligible diffusion from the holes into the gaps around the filaments along the edge of the ply. After filling the gaps around the filaments along the edge of the ply, this region of the hole wall is considered to be a flat surface on which deposition occurs, reducing the dimension of the hole. The surfaces of each ply are assumed to be flat. The error in surface area due to neglecting overlapping of tows should be negligible, because the thickness of a tow is very small. The effect on the diffusion coefficient due to the uneven surface is accounted for by a tortuosity factor of $\sqrt{2}$.

The hole is divided into two parts: one part is the hole wall along the edge of the ply (distance, c_n) where deposition occurs, and the other part is the open space between plies of distance, b_n, where diffusion takes place into the x and y regions between plies (Figure 2). Deposition starts on the hole wall, along distance c_n, after the gaps are filled around the outer filaments. Before the gaps around the filaments at the boundary between the hole and the next ply are plugged, the depth of a hole, h_n, is h_o. After those gaps are filled, h_n decreases due to the deposition at the bottom of the hole. Deposition on the flat surface of one ply starts after the gaps around the outer filaments are filled with deposit. Before these gaps are filled, the mass balance in the spaces between plies includes diffusion on both sides of a ply. After filling the gaps around the outer filaments, deposition occurs on the flat surfaces of the upper and surfaces of the lower plies. In the gaps, deposition occurs on the outside surface of the cylindrical filaments. Deposition in the gaps in each ply stops when the radius of outer filaments is equal to r_p, the plugging radius. The procedure for evaluating r_p is explained previously (Chung et al., 1992).

The model is developed by solving mass-balance equations for gas-phase concentrations of reactants DDS and $TiCl_4$ for the three parts of the system (holes, spaces, and gaps) combined with equations for the change with time of the dimensions of the system. Mass-balance equations for each component are the same as shown in the previous article (Chung et al., 1992), except that one more suffix is needed to identify the reactant species. Two sets of mass-balance equations, one set for DDS and the other for $TiCl_4$, are solved.

For case III, the precursors enter sequentially in the feed with compositions given in Table 1. When one component is

switched to the other, it is assumed that effects of the leftover amount of the previously changed component are small compared to the deposition of that component during the time interval. Hence, the concentrations inside the sample of the previously fed reactant are assumed to be zero when the other reactant enters the sample.

Change of dimensions with time

The concentration profiles in the voids change with dimensions of the system: the side length of the hole, distance between plies, thickness of the ply, and radius of the filament. These dimensions change with time due to depositions of TiB_2 and SiC, and are expressed by the mass-balance equations that follow.

The rate of change of the dimension of the hole is:

$$\frac{\partial a_n}{\partial t} = -2\left(\frac{q_S M_{mS}}{\rho_{mS}} k_S C_{z'\,S,n} + \frac{q_T M_{mT}}{\rho_{mT}} k_T C_{z'\,T,n}\right) \tag{1}$$

$$\text{i.c} \quad a_n = a_o \quad \text{at} \quad t \le t_{a,n} \tag{2}$$

For the hole wall along the edge of the ply, t_a is the time required to plug the gaps around the outer filaments at the edge of a ply. For the open space of the hole along the distance b_n, t_a is the time required to occlude the space between plies at the entrance from the hole.

The rate of change in the depth of the hole is:

$$\frac{\partial h_n}{\partial t} = -\left(\frac{q_S M_{mS}}{\rho_{mS}} k_S C_{z'\,S,n}|_{z'=h_n} + \frac{q_T M_{mT}}{\rho_{mT}} k_T C_{z'\,T,n}|_{z'=h_n}\right) \tag{3}$$

$$\text{i.c.} \quad h_n = h_o \quad \text{at} \quad t \le t_{h,n} \tag{4}$$

Here, $t_{h,n}$ is the time required to plug the gaps around the outer filaments at the boundary between the hole and the next ply.

The equation for the change of distance between plies is:

$$\frac{\partial b_{n,i,j}}{\partial t} = -2\left(\frac{q_S M_{mS}}{\rho_{mS}} k_S C_{x\,S,n,i,j} + \frac{q_T M_{mT}}{\rho_{mT}} k_T C_{x\,T,n,i,j}\right) \tag{5}$$

$$\text{i.c.} \quad b_{n,i,j} = b_o \quad \text{at} \quad t \le t_{b,n,i,j} \tag{6}$$

Here, $t_{b,n,i,j}$ is the time required to plug the gaps around the filaments at the outer surface of a bundle of filaments (tow) at position (x_i, y_j). Note that these gaps at the outer surface may be plugged while voids still exist around the inner filaments in the bundle resulting in incomplete densification. The equation for the change of thickness of a ply is:

$$\frac{\partial c_n}{\partial t} = -\frac{1}{2}\left(\frac{\partial b_{n,i,j}}{\partial t}\bigg|_{x=0} + \frac{\partial b_{n-1,i,j}}{\partial t}\bigg|_{y=d_o/2}\right) \tag{7}$$

$$\text{i.c.} \quad c_n = c_o \quad \text{at} \quad t \le t_{b,n,l,j} \tag{8}$$

Again, $t_{b,n,l,j}$ is the time required to plug the gaps around the filaments at the outer surface of a ply.

The rate of change of the radius of a filament is given by the mass balance:

$$\frac{\partial r_{n,i,j,k}}{\partial t} = \frac{q_S M_{mS}}{\rho_{mS}} k_S C_{z''\,S,n,i,j,k} + \frac{q_T M_{mT}}{\rho_{mT}} k_T C_{z''\,T,n,i,j,k} \tag{9}$$

$$\text{i.c.} \quad r_{n,i,j,k} = r_o \quad \text{at} \quad t = 0 \tag{10}$$

The method of solution of these equations is first to calculate the concentration profiles at a given time in the holes, spaces between plies, and gaps around the filaments, employing the pseudo-steady-state equations (Chung et al., 1992). Then, the change in dimensions for a chosen time increment is calculated using Eqs. 1-10 with the calculated concentration profiles. This procedure is repeated for successive time increments to yield concentration profiles and dimensions of the system as a function of time. From these results, deposition amounts and porosities are evaluated. Changes in dimensions due to depositions of SiC and TiB_2 can be obtained separately for each time increment. With these changes in dimensions due to each component, the amount of deposition of each component in the deposit also can be calculated.

The equations were first made dimensionless and then solved numerically in finite-difference form with 50 nodal points in the z' direction in the hole, 10×10 nodal points in x and y directions in the space, and five nodal points in the z'' direction in the gaps. The smaller number of nodal points in the space between plies and gaps around filaments was chosen to obtain a reasonable computing time without sacrificing accuracy and a time comparable to that for the single-component deposition calculation in the staggered-hole model. A time increment of 2 min was chosen for processing times. All the calculations were done with either FPS264 or Cray Y-MP supercomputers, requiring about 2.5 h FPS cpu time and about 25 min Cray cpu time for a typical run. The complex substrate geometry and multiple operating parameters lead to extensive numerical data. For brevity, illustrative results are displayed only for gas-phase concentrations, deposit compositions, and overall porosities, primarily as a function of time.

Results and Discussion

Dimensions and deposition conditions for dispersed and graded deposition

Table 1 lists initial substrate dimensions and deposition conditions used to compare results for the three operating procedures (cases 1, 2, and 3). The dimensions are measurable quantities in a particular system. At the reaction conditions in Table 1, the first-order reaction rate constant for SiC deposition, k_s of 10 cm/min (Chung et al., 1992), was used. Besman and Spear (1977) measured the deposition rate of TiB_2 from $TiCl_4$, BCl_3, and H_2 as 0.5 mg/cm^2·min at 925°C. Using this value and the concentration of BCl_3 employed in their experiment, the equivalent first-order reaction rate constant (based on $TiCl_4$) for TiB_2 deposition, k_T, was estimated as 35 cm/min.

Effective diffusion coefficients in the space between plies and in the gaps around filaments were obtained in the same way as mentioned in the staggered-hole model (Chung et al., 1992). The effective diffusion coefficient in the uneven space between plies was estimated using a tortuosity factor $\sqrt{2}$. The effective diffusion coefficient in the gaps around the filaments was estimated from the porosity and the initial tortuosity factor, κ_o, according to the equation $D_{eg} = D_{mk}\,\epsilon/\kappa_o$. Since the

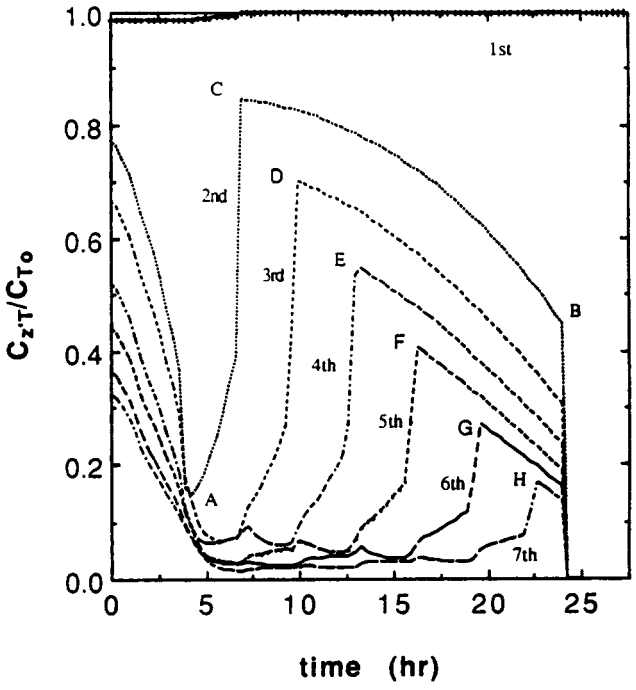

Figure 3. Concentration of $TiCl_4$ vs. time in the middle of each hole with parameter values in Table 1.

This is for case I, simultaneous feed of constant composition. *A* is the time of plugging gaps around the outer filaments of the sample; *B*, the time of plugging the first space; *C*, *D*, *E*, *F*, *G*, and *H* are times of plugging gaps around the outer filaments at the ply surfaces in the 1st, 2nd, 3rd, 4th, 5th and 6th space.

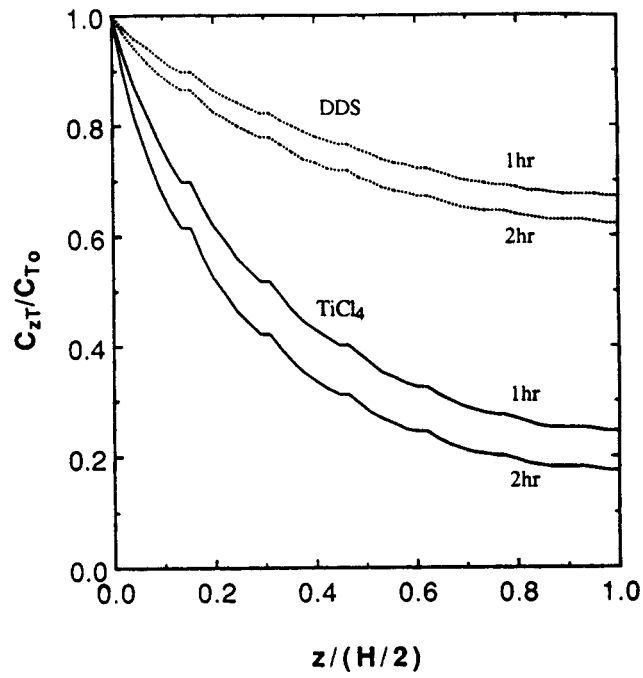

Figure 4. Concentration profiles of $TiCl_4$ and DDS for case I along the *z* axis in the middle of each hole at 1 and 2 h (following the line connecting points of U and V in Figure 2).

dimensions of the voids may be very small, the temperature high, and the pressure low, Knudsen diffusion was included in obtaining effective diffusion coefficients in the gaps around the filaments. The parameter values in Table 1 are based on the geometries for a typical substrate fabricated at the NASA Ames Research Center and used to compare results for the three operating procedures.

Gas-phase concentration profiles

The general trend of concentration change with time is similar to that for single-component deposition. Hence, only a few illustrations are shown. The concentration of $TiCl_4$ for case I (simultaneous deposition) in the middle of each hole is shown in Figure 3. All the curves decrease at low times because of increasing reactant depletion caused by increasing surface area around filaments. Also, there is a drop in concentration (point A in Figure 3) when the gaps around the outer filaments of the sample are plugged, because the diffusion flux into the gaps around filaments from the outside of the sample ceases after this time. The first hole becomes the only passage for diffusion into the sample from outside. After this concentration drop, the concentration in the second hole increases as the gaps around the outer filaments at the ply surfaces in the first space are progressively plugged. During this time the concentrations in the deeper inside of the sample drop a little, due to less diffusion through the gaps around filaments in the second ply. The point C in Figure 3 is the time that gaps around the outer filaments at the ply surfaces in the first space (space between plies one and two) are plugged completely. At this

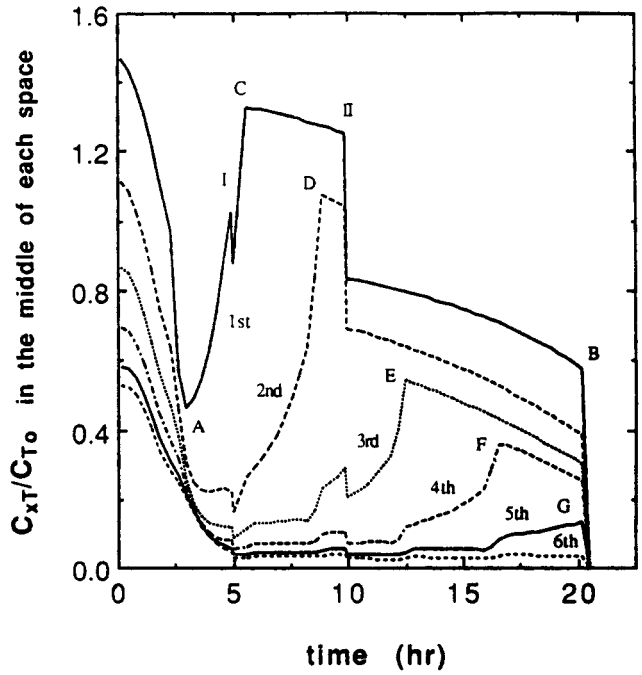

Figure 5. Concentration of $TiCl_4$ vs. time in the middle of each space for case II, graded deposition with changing feed composition.

A, is the time of plugging gaps around the outer filaments of the sample; B, time of plugging the first space; C, D, E, F, and G, times of plugging gaps around the outer filaments at the ply surfaces in the 1st, 2nd, 3rd, 4th, and 5th space. I (5 h) and II (10 h) are the times that concentrations in the feed are changed.

time, the inner concentrations increase. After plugging the gaps around the outer filaments at both sides of first ply and the upper side of second ply, the concentration in the third hole starts increasing as the gaps around the outer filaments at the ply surfaces in the second space are progressively plugged. During this time, concentrations in the inner side of the sample drop a little due to the decreasing diffusion flux through gaps around filaments in the third ply. The point D in Figure 3 is the time that gaps around the outer filaments at the ply surfaces in the second space are plugged completely. At this time, the inner-side concentrations increase again. The concentration curves in the 3rd, 4th, 5th, and 6th spaces also behave in the same way. Similarly, the points E, F, G and H are the times that gaps around the outer filaments at both ply surfaces in the 3rd, 4th, 5th, and 6th spaces are plugged completely. After points C, D, E, F, G and H, the concentrations in the holes decrease as the distances between plies become smaller due to deposition. Finally, all the inside concentrations, except the concentration in the first hole, become zero when the first space is plugged (point B in Figure 3).

Figure 4 shows the concentration profiles of $TiCl_4$ and DDS along the z axis at one- and two-hour reaction times for case 1. Since it is assumed that there is no concentration gradient in the very small distance in the z direction in the space between plies, the concentration profile shows a steplike curve. The distance between plies is one tenth the thickness of a ply. Hence, the flat portions of the curve are very narrow. Distribution curves of DDS are flatter than those for $TiCl_4$ because of the larger diffusion coefficient (2.7 times) for DDS, as shown in Table 1. The significant gradients in Figure 4 show that, for the geometry chosen, diffusion within the sample affects the reactant concentrations.

For case II (deposition with changing feed concentrations as given in Table 1), the concentration of $TiCl_4$ in each *space* is shown in Figure 5. Points A, B, C, D, E, and F have the same meaning as in Figure 3. Point H in Figure 3 does not exist in Figure 5. This means that until the first space is plugged, the gaps around the outer filaments of the 7th ply are not plugged. Hence, deposition in the gaps around filaments in the 7th ply is continued until the first space is plugged. Here, points I (5 h) and II (10 h) are the times when concentrations to the sample are changed.

For case III, deposition with a sequential feed of reactants, the results are similar to those for case II (Figure 5) except that for the time intervals when only BCl_3, not $TiCl_4$, is supplied to the sample. The concentrations increase after the drop at low times because, as before, the gaps around the outer filaments become plugged. Case III represents severe changes in feed composition and, therefore, could be considered as an extreme illustration of the more general case II.

Deposit properties

Figures 6 and 7 give the amount of deposition of TiB_2 and SiC in the gaps around the filaments in each ply as a function of time. Figures 8 and 9 show the amount of deposition in the middle of each space between plies. Letters A to H correspond to the same times, as described for Figure 3. Thus, A is the time when the gaps around the outer filaments of the sample are plugged, and C is the time when the outer filaments in the first space between the plies are plugged. When the outer filaments in the spaces between plies are plugged, deposition in the gaps ceases as noted by the horizontal lines in Figures 6 and 7. This occurs at increasing times going into the sample since the gaps around the filaments in the first ply plug first, second ply next, and so on. As shown in Figure 2, only half of the 7th ply is considered so that the volume of gaps around

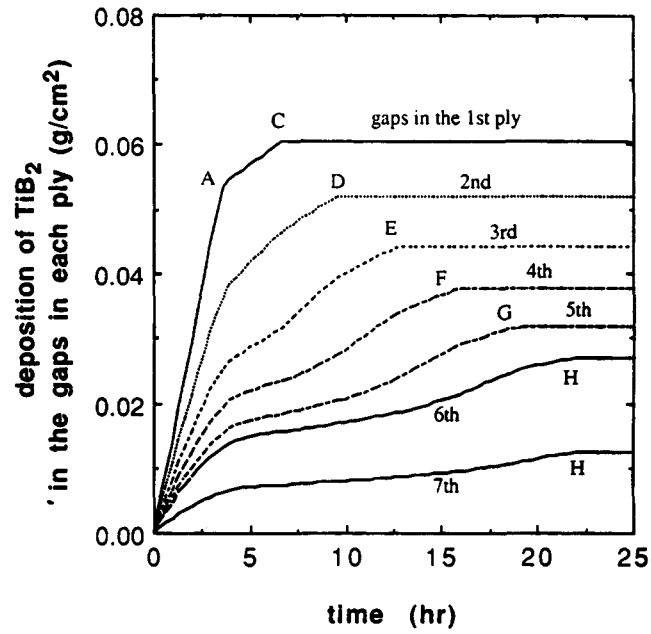

Figure 6. Deposition of TiB_2 (g/cm^2 of cross-sectional area of sample) in the gaps around the filaments in successive plies of the sample (case I).

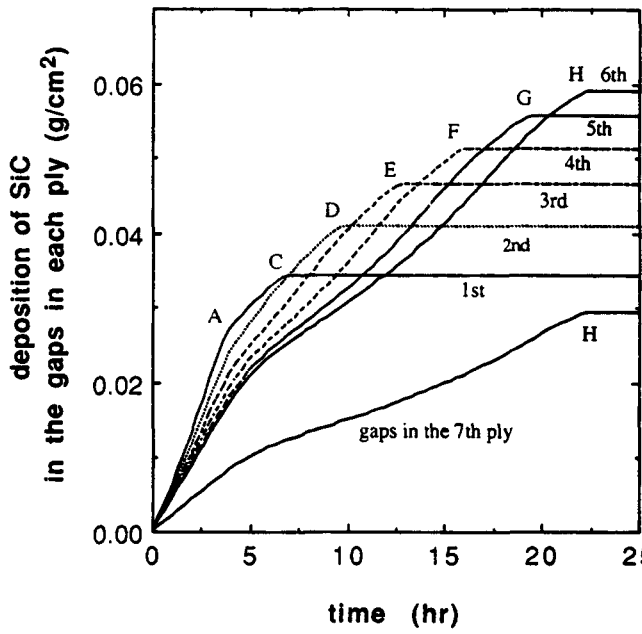

Figure 7. Deposition of SiC (g/cm^2) in the gaps around the filaments in successive plies of the sample (case I).

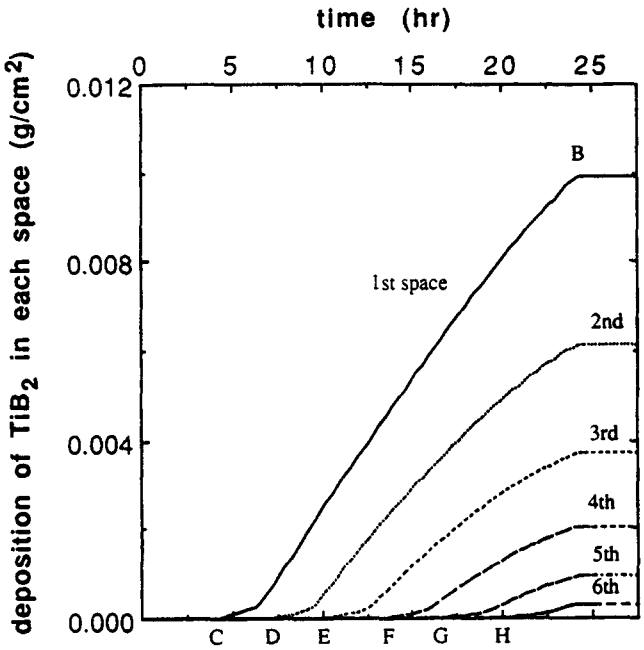

Figure 8. Deposition of TiB_2 (g/cm^2) in the spaces between successive plies of the sample (case I).

filaments in the 7th ply is less than on the other plies and about half that in the 6th ply. In the first ply, gaps around the filaments are directly available to the outside of the sample. Hence, effects of diffusion on the concentrations in the gaps around filaments in the first ply are minimal. The amount of deposition in the first ply depends mainly on the feed concentration and deposition rate constant. As shown in Table 1, the feed concentration of DDS is 2.4 times that of $TiCl_4$. The rate constant for SiC deposition, however, is less than one third that of TiB_2 so that the final amount of deposition of SiC in the gaps around the filaments in the first ply (Figure 7) is only 0.57 times that of TiB_2 (Figure 6). Going into the sample, the final amount of deposition of SiC in the gaps around filaments in each ply increases and that of TiB_2 decreases. The difference is mainly because the diffusion coefficient of DDS is 2.7 times that of $TiCl_4$. As a result, the concentration profiles of DDS along the z axis in the sample become higher (3 times in the middle of the sample) than those of $TiCl_4$, as shown in Figure 4. After the outer gaps in the first ply are plugged, the concentration profile of DDS becomes much higher (4 times in the middle of the sample) than that of $TiCl_4$ at the inner side of the sample. Therefore, even though the deposition rate of SiC is low, the higher concentration of DDS in the gaps in the inner plies makes the final amounts of deposition there more than those in the outer plies, as shown in Figure 7. In contrast, the lower concentrations of $TiCl_4$ in the gaps in the inner plies result in smaller amounts of deposition of TiB_2, as shown in Figure 6. Hence, going into the sample (increasing ply number), the deposition of SiC in the gaps around the filaments increases while the opposite occurs in TiB_2. The ratio of SiC to TiB_2 deposit in the gaps around filaments in each ply changes from 0.57 for the first ply to 2.32 for the 7th ply. Deposition amounts in the gaps and in the spaces between plies are summarized in Table 2.

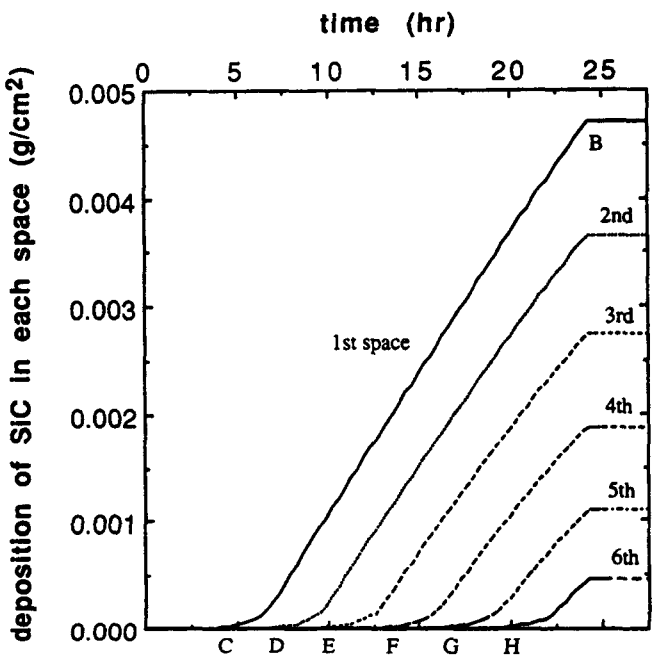

Figure 9. Deposition of SiC (g/cm^2) in the spaces between successive plies of the sample (case I).

Table 2. Deposition of SiC and TiB_2 in the Gaps around Filaments in Each Ply and in the Spaces between Plies, per Unit Cross-Sectional Area of the Sample, at the Time of Plugging of the First Space: Case I

Ply	Amount of Deposition* SiC	TiB_2	Total	Ratio of SiC/TiB_2
In the Gaps around Filaments of Each Ply				
1st	0.035	0.060	0.095	0.57
2nd	0.041	0.052	0.093	0.79
3rd	0.047	0.044	0.091	1.06
4th	0.051	0.038	0.089	1.36
5th	0.056	0.032	0.088	1.76
6th	0.059	0.027	0.086	2.19
7th	0.029	0.013	0.042	2.32
In Each Space Between Plies				
1st	0.0047	0.0100	0.0147	0.47
2nd	0.0037	0.0061	0.0098	0.60
3rd	0.0027	0.0037	0.0064	0.73
4th	0.0019	0.0020	0.0039	0.95
5th	0.0011	0.0009	0.0020	1.22
6th	0.00045	0.0003	0.00075	1.50

*g/cm^2 cross-sectional area of the sample.

Figures 8 and 9 show the amount of deposition in the middle of each space between plies. The spaces between the first ply become plugged after a longer time, as noted in Figures 8 and 9. This time is nearly the same for all plies because no deposition in subsequent plies can occur after the first space (between plies one and two) becomes plugged. The low values of the amount deposited for the interior plies, as shown in Figures 8 and 9, mean that there will always be some residual porosity in the center section of the sample. This result has serious

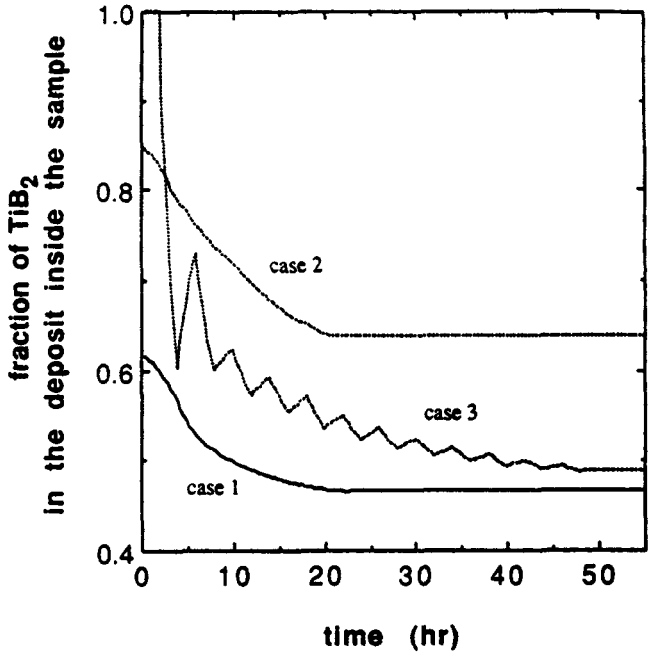

Figure 10. Composition of the overall deposit for cases I, II and III.

consequences for the mechanical properties and oxidation resistance of the composite.

The composition of the deposit is indicated in Figure 10 for the three cases. The fraction TiB_2 is low for case I, since DDS has a larger diffusivity and its concentration in the feed gas is higher, more than offsetting the larger rate constant for TiB_2 deposition (Table 1). In contrast, the deposit contains more

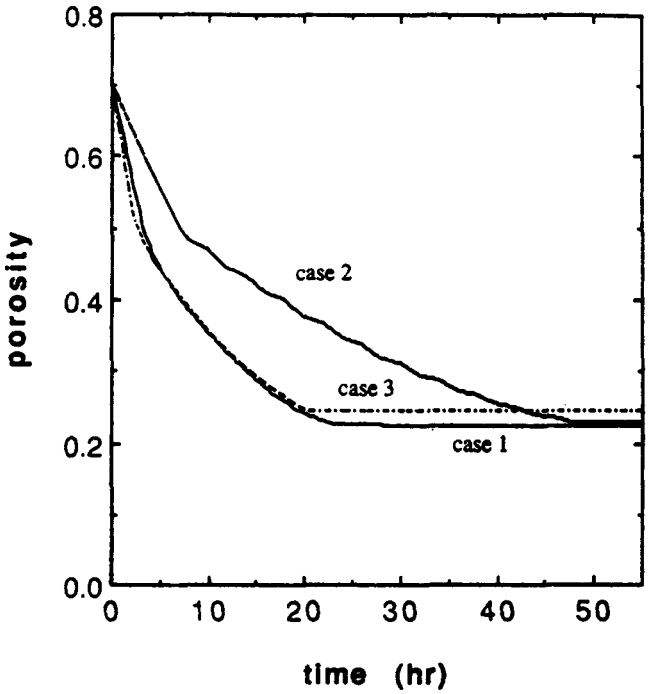

Figure 11. Overall porosities of the sample for cases I, II and III.

Table 3. Parameter Values for Sensitivity Calculations

Kinetic Model

$$\frac{d\mathrm{TiB_2}}{d\theta} = A_T e^{-E_T/RT} C_{\mathrm{TiCl_4}} \qquad \frac{d\mathrm{SiC/Si}}{d\theta} = A_S e^{-E_S/RT} C_{\mathrm{DDS}}$$

Kinetic Constants

A_T(cm/min)	E_T(cal/mol)	A_S(cm/min)	E_S(cal/mol)
6.9475×10^8	40,000.0	1.6217×10^9	45,000

Rate constant @ 1,198 K, 1.32×10^3 Pa

35 cm/min (1% $TiCl_4$) 4.17 cm/min (1% DDS)

Molecular Diffusion Coefficient (cm^2/min) @ 1,198 K, 1.32×10^3 Pa	$TiCl_4$	DDS
	6,700	17,900
Density (g/cm^3)	TiB_2	SiC
	4.5	3.2

	Fabric A	Fabric B
Side of Hole (cm), a_o	0.06	0.034
Ply Thickness (cm), c_o	0.024	0.008
Radius of a Filament (cm), r_o	0.0004	0.0003
No. of Plies, N	13	13
Distance between Plies (cm), b_o	0.003	0.0015
Width of Tow (cm), d_o	0.18	0.098
No. of Filaments in a Tow	3,000	1,000
Total Height of Samples (cm)	0.348	0.122
$\left[\frac{\text{No. of Filaments}}{\text{Unit Cross-Sectional Area}}\right]$ (cm^{-2})	6.95×10^5	12.63×10^5
Initial Tow Porosity	0.6509	0.6430
Initial Porosity	0.7066	0.7149
Plug Radius (cm), r_p	0.000645	0.000478
r_p/r_o	1.6119	1.5933
$r_p - r_o$ (cm)	0.000245	0.000178

TiB_2 than SiC for case II, since the feed gas contains more $TiCl_4$ during the 0–5 h time period when most of the deposit is produced (Figure 6). Case II shows the results for a graded deposit, and comparison with case I displays the flexibility in deposit composition that can be achieved by varying the gas mixture fed to the sample. Such predictions are useful for designing operating procedures for optimum properties of the resultant composites.

Porosity

Figure 11 shows the overall porosity (sum of void volume in the gaps, spaces, and holes divided by total volume of the sample) for the three cases. Porosities are nearly the same for simultaneous (case I) feed gas of 2.4% DDS and 1.0% $TiCl_4$ and sequential feeds (Case III) of 2.4% DDS followed by 1.0% $TiCl_4$. However, graded composites (case II) where the feed gas initially contains more $TiCl_4$ have larger porosities up to about 40-h reaction time. This is because the density of TiB_2 is greater than that of SiC. While only average porosities are given in Figure 11, an advantage of our discrete model is that porosities in all parts of the sample, in the gaps around filaments, spaces between plies, and holes through the plies, are available at any reaction time. The prior article (Chung et al., 1992) gives porosities for the deposition of only SiC for the same sample dimensions and deposition conditions, except that the feed contained 3.75% DDS rather than 2.4%. The porosity curve for SiC alone is somewhat lower than that for case I in Figure 11 and ends with an asymptotic value of about 0.17.

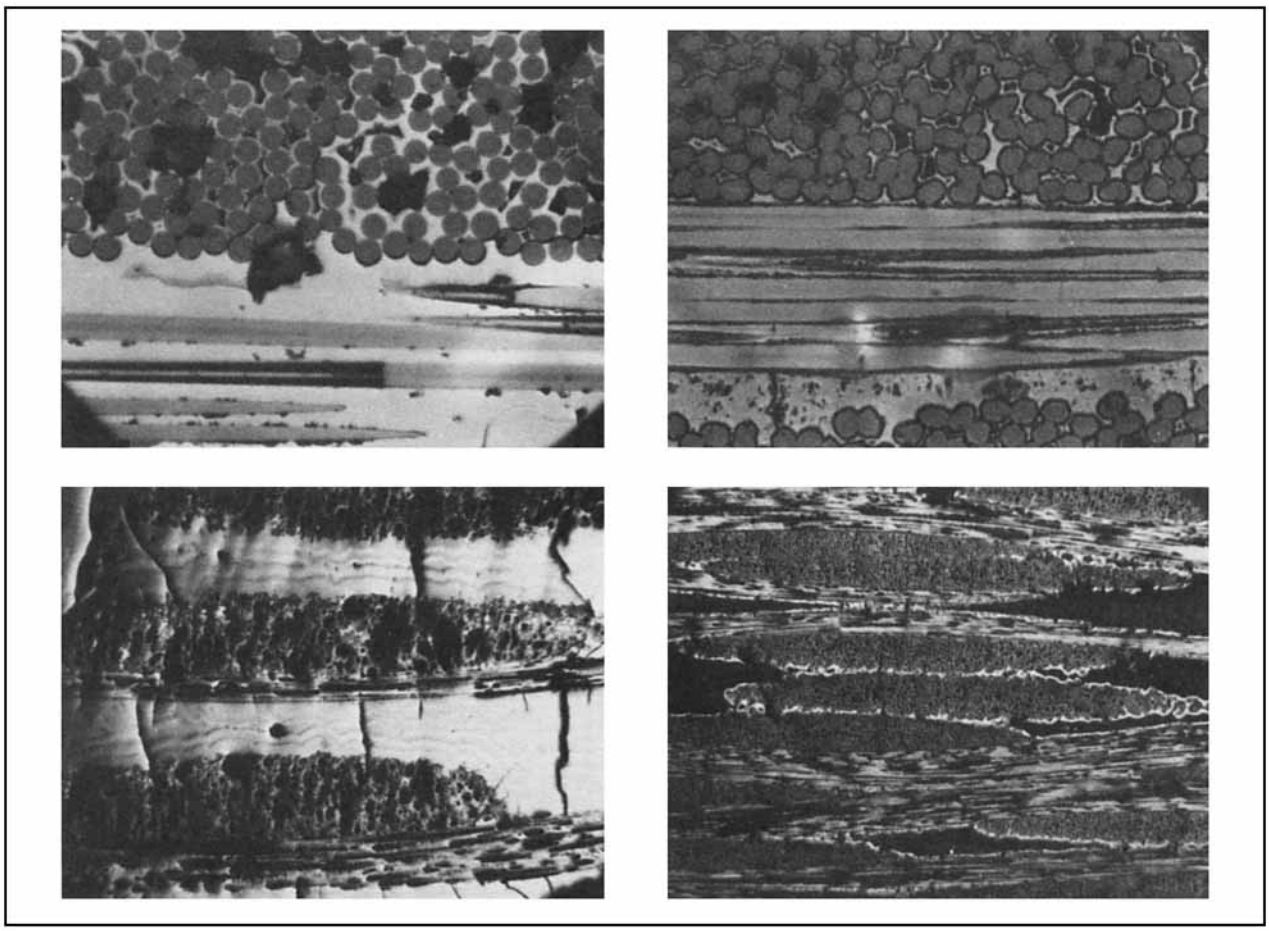

Figure 12. Photomicrographs of infiltrated fabrics A and B.

Magnification 628× (upper photos) and 78× (lower photos).

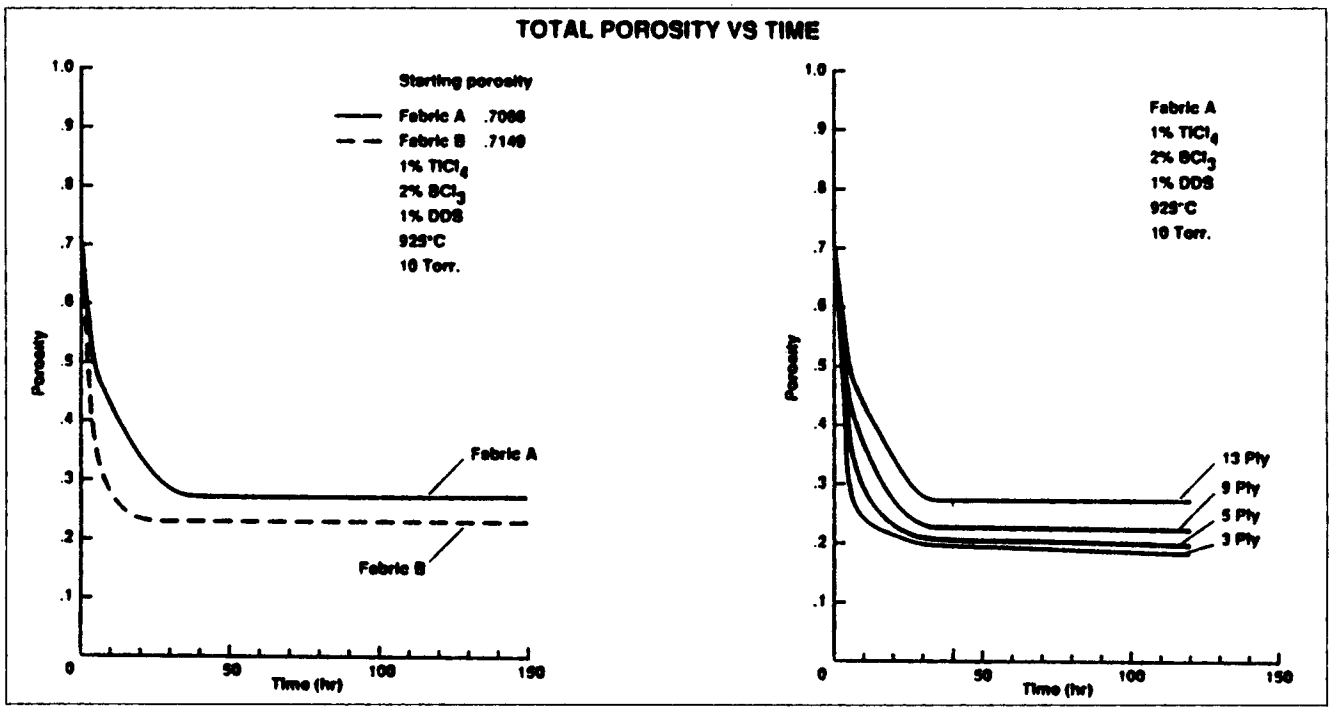

Figure 13. Overall porosity vs. time for fabrics A and B (and as a function of a number of plies for fabric A).

Table 4. Effect of Temperature on Final Porosity (Fabric A, 13 Plies)

Temp. (°C)	Pres. (torr)	$TiCl_4$ (Vol.%)	DDS (Vol.%)	Final Porosity
925	30	1	1	0.3076
1,000	30	1	1	0.4554
925	30	0.1	1	0.2118
1,000	30	0.1	1	0.3407
925	30	1	0.1	0.3989
1,000	30	1	0.1	0.5281

The higher porosity for simultaneous deposition of both SiC and TiB_2 is due to the more rapid plugging of the outer gaps around the filaments, thus enclosing more void spaces through the sample. Similar results where the holes in successive plies are aligned (Chung et al., 1991) show even lower porosities, because plugging spaces between outer plies do not hinder access to interior plies. Denser composites are possible if the fabric is woven to allow unconstrained access to interior plies.

Effects of input parameters (sensitivity analysis)

For the effects of temperature, pressure and reactant gas composition, results were obtained for two substrates, A and B, of different geometry as described in Table 3. This table also lists molecular diffusivities, kinetic constants, and solid densities (of TiB_2 and SiC) used in these sensitivity calculations, which were for simultaneous feed compositions (case I) of the reactants.

Figure 12 shows cross sections for infiltrated 13-ply substrates of fabrics A and B. The two substrates exhibit quite different geometries. In fabric B, the filaments in the tows appear crenelated and more closely and regularly packed. More detailed examination shows that the diameter of the filaments, the size of the holes, the width of the tows, the thickness of the plies, the number of filaments in a tow, and the space between adjoining tows (ply spacing) are smaller than those in fabric A. These differences in substrate configuration may prove important and influence the progress of mass transfer, chemical reaction, and deposition, especially with respect to being able to infiltrate the substrate with a uniform and/or controlled porosity and composition.

Figure 13a displays the overall porosity predicted as a function of time. Fabric B is more fully infiltrated and has a final porosity about 5% lower than fabric A at 925°C and 10 torr. Decreasing the tow width, ply thickness, and height of the 13-ply sample provides better access to the interior plies resulting in more complete infiltration (fabric B). In Figure 13b, the porosity is shown as a function of the number of plies in a layup for fabric B. Porosity increases as the number of plies increases due to the increase in thickness and diffusion path.

The effect of temperature on final porosity is shown in Table 4 for 925°C and 1,000°C and three reactant gas compositions. The significant increase in final porosity with temperature is due to the increase in deposition rates with respect to diffusion rates. This causes more rapid plugging between the outer plies and results in less infiltration into the inner plies.

The plots in Figure 14 show the amount of SiC deposited in the spaces between plies and within the plies for fabric A. The first space between plies plugs at about 32 h. This is a

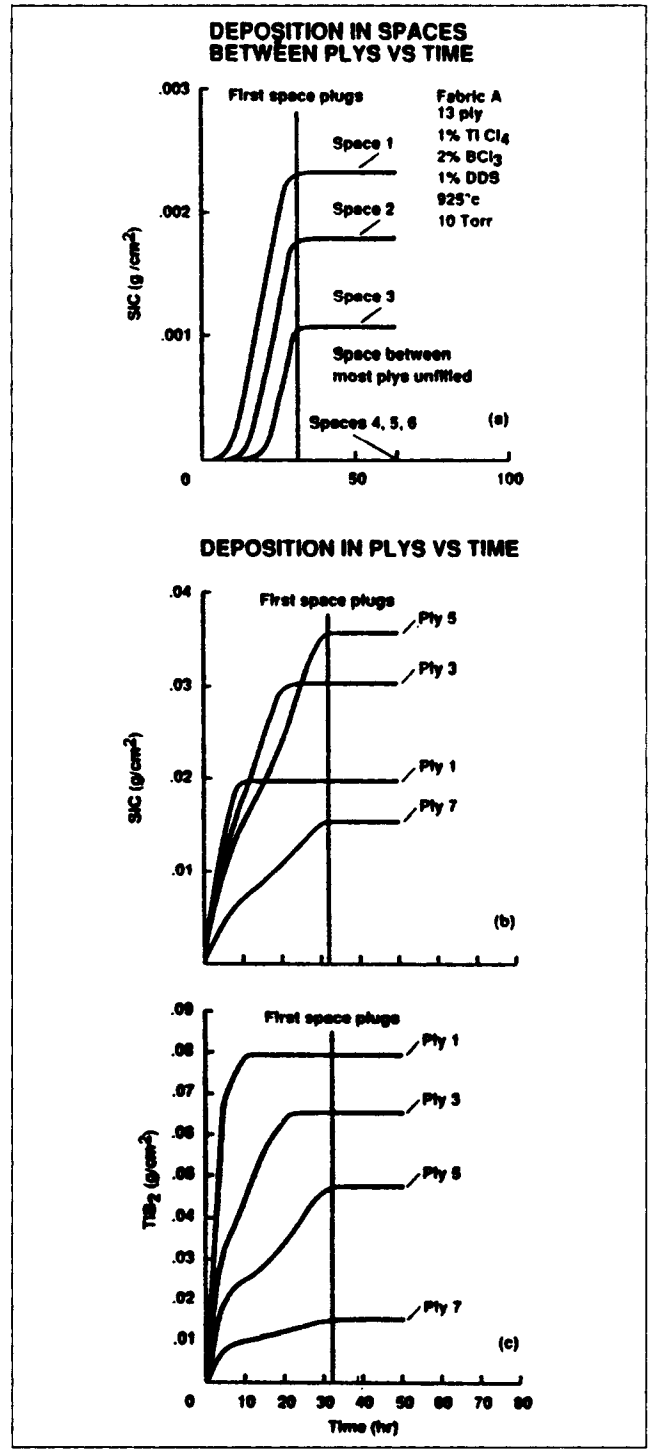

Figure 14. Deposition amounts of SiC and TiB_2 for fabric A.

critical factor restricting deposition in between the filaments and spaces in the innermost plies. Similar information is shown in Figure 15 for fabric B. Here, all the plies and spaces contain considerable deposit, even before the first space plugs (the relative properties of the tows, thickness, and ply spacing allow greater in-depth deposition). Aside from the thickness of the

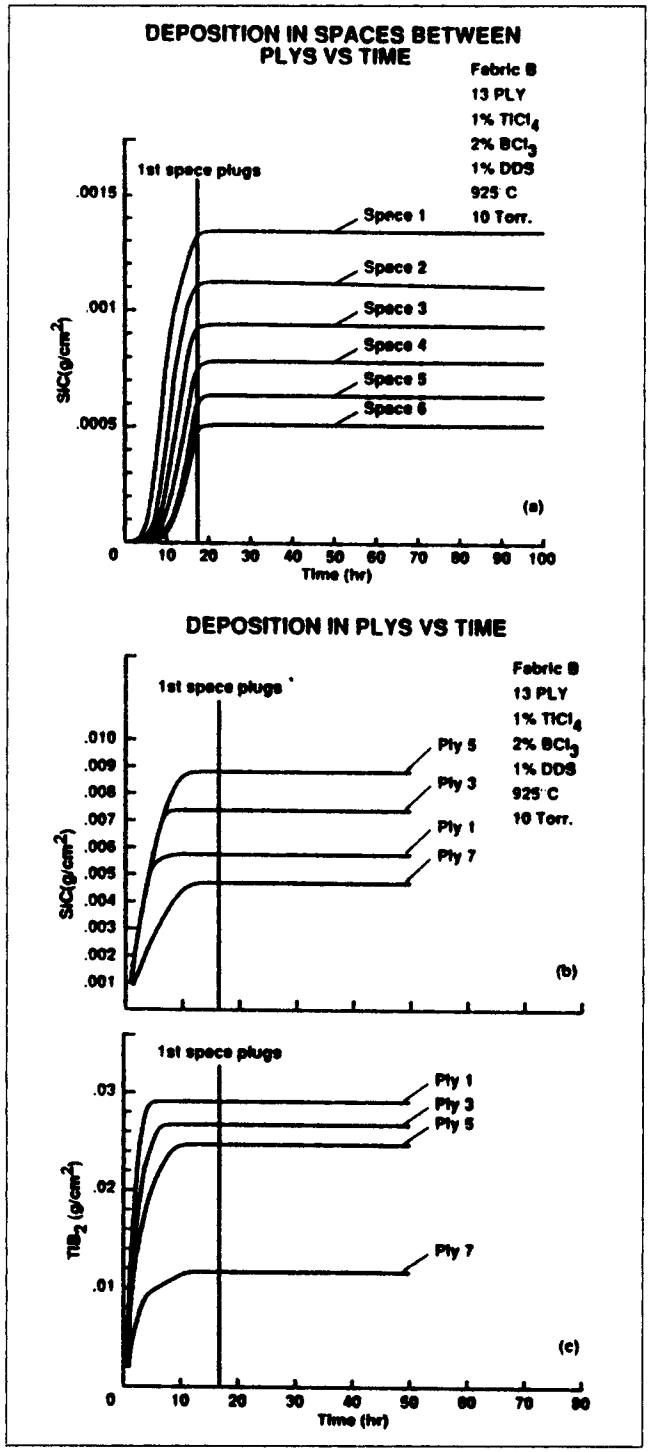

Figure 15. Deposition amounts of SiC and TiB_2 for fabric B.

fabric B being smaller, each outer ply also has fewer filaments (1,000 vs. 3,000) to act as a "sink" for deposition.

In Figure 14, it is apparent that some inner spaces between plies in fabric A have no deposit at all (there can be little bonding between these plies). For fabric B (Figure 15), there is some deposit and potential bonding between all of the plies. This result has obvious and major consequences on the mechanical properties and oxidation resistance of the composite. Plies which have poor bonding are prone to delaminate. Areas in which a protective coating does not exist are subject to oxidation.

Table 5. Final Porosity vs. Time—1% $TiCl_4$, 2% BCl_3, 1% DDS at 1,198 K Fabric A-13 Ply

Pres. (torr)	Final Porosity	Time (h)
1	0.2703	274.3
1	0.5449	36.9
10	0.2737	36.9
30	0.3076	36.9
100	0.3462	36.9
228	0.3623	22.2
760	0.4231	6.72

Table 5 shows final porosity as a function of pressure for 925°C. Reducing the pressure has a marked effect on diffusion, allowing material to diffuse faster and deposit in depth before the first space and tow are plugged and create a barrier. Therefore, decreasing the pressure decreases the final porosity. The data in the table also suggest that, if all factors are the same, little is gained by decreasing the pressure from 1.32×10^3 to 1.32×10^2 Pa (10 to 1 torr). The efficiency of the process decreases with respect to time at the lower pressure. The time necessary to reach almost equivalent final porosities for a pressure of 1 torr is a factor of 10 greater than at 10 torr. This is due to the decrease in the deposition rate which accompanies the decrease in pressure. Decreasing the pressure increases the diffusion rate but decreases the reaction rate since the concentration of reactants is proportional to pressure.

Conclusions

The structured geometry model (Chung et al., 1992) predicting chemical vapor infiltration in various sections of plies of woven tows of carbon carbon filaments has been applied to combined deposition of two components. Results for a typical fabric are given for deposits of SiC plus TiB_2 when the concentration of the gaseous precursors changes with time (graded deposits) and when dispersed deposits are produced by simultaneous feed gases of constant composition or sequential feeds yielding SiC and then TiB_2. The model predicts gas-phase concentrations, deposit amount and porosities in the three sections of the samples (gaps, spaces, and holes), all as a function of time. For the same conditions, densification (overall porosity) is about the same for all three cases at long reaction times. During the earlier stage of deposition, however, lower densification is predicted for the simultaneous feed of both precursors. These results are for a staggered arrangement of the holes between successive plies of the sample. This leads to lower final densification than when the holes are aligned, due to plugging of the spaces between plies.

The model was also applied for two fabrics of different geometry. Due to plugging of voids around the filaments and in the spaces between plies, initial geometry (such as number of filaments per tow, diameter of filament, and space between plies) can greatly affect not only overall porosity but porosity distribution. For one fabric of typical geometry, it is shown that inner plies can be devoid of deposition while spaces between outer plies are completely plugged. This condition can

have adverse consequences on the mechanical properties and oxidation resistance of the composite.

Results of sensitivity analysis show that the time required to obtain the same final porosity increases sharply with decrease in pressure even though diffusivities increase. The effect of increasing the temperature is to increase final porosity.

Acknowledgment

This work was supported by NASA Cooperative Agreement NCC 2-590. The authors are grateful for the computer time provided by the University of California, Davis, Computer Center and the University of California, San Diego Supercomputer Center.

Notation

a = side length of the square hole, cm
b = distance between plies, cm
c = thickness of one ply, cm
C_o = concentration of reactant at the outside of the sample, mol/cm^3
C_x = concentration of reactant along the x and y axes in the space between plies, mol/cm^3
C_z = concentration of reactant along the z axis in the sample, mol/cm^3
$C_{z'}$ = concentration of reactant along the z axis in the hole, mol/cm^3
$C_{z''}$ = concentration of reactant along the z axis in the gaps, mol/cm^3
$C_{z'H}$ = concentration of reactant along the z-axis in the gaps connected with a hole, mol/cm^3
d = distance between holes, width of tow, cm
D_{eg} = effective diffusion coefficient in the gaps around the filaments, cm^2/min
D_{es} = effective diffusion coefficient in the space between plies, cm^2/min
D_k = Knudsen diffusion coefficient, cm^2/min
D_m = molecular diffusion coefficient, cm^2/min
D_{mk} = composite diffusion coefficient, cm^2/min
g = diffusion distance in the ply when the upper side of a ply is plugged, cm
h = height of the hole, cm
H = total height of the sample, cm
k = first-order reaction (deposition) rate constant based on deposition rate, cm/min
M_A = total number of divisions along the side-length of the hole ($=a_o/\Delta x$)
M_B = total number of divisions in the x and y directions in the space ($=d_o/2\Delta x$)
M_m = molecular weight of deposit, g/mol
N = total number of plies
N_x = flux of diffusion in the x and y directions, mol/cm$^2\cdot$min
$N_{z''}$ = flux of diffusion in the z'' direction, mol/cm$^2\cdot$min
p = average porosity of the whole sample
q = number of deposited molecule per molecule of reactant
r = radius of a filament, cm
r_H = radius of a filament in the part of a ply connected with a hole, cm
R = radius of average void opening between filaments, cm
s = surface area of the filaments per unit volume of the ply, cm^2/cm^3
S = number of holes in unit cross-sectional area, cm^{-2}
t = time, min
t_a = time required to plug the gaps around the outer filaments at the hole-edge of a ply, or time required to plug the space between plies at the entrance from the hole at position z; $t_a=f(z')$, min
t_b = time required to plug the gaps around the outer filaments at position x; $t_b=f(x)$, min
t_h = time required to plug the gaps around the filaments at the boundary between the hole and the next ply, min
T = number of spaces or plies of length d_o in unit cross-sectional area, cm^{-2}
W = number of filaments per unit cross-sectional area perpendicular to the axis of the filaments, cm^{-2}
x, y = coordinates in the direction of diffusion in the space between plies, cm
z = coordinate in the direction of diffusion in the sample, cm
z' = coordinate in the direction of diffusion in the hole, cm
z'' = coordinate in the direction of diffusion in the gaps around the filaments, cm

Greek letters

ϵ = local porosity of a ply
κ = tortuosity in the gaps around the filaments
ρ_m = density of the deposited material, g/cm^3
Φ = amount of deposition, g/cm^2 of cross-sectional area of sample

Subscripts

i = ith segment of a space or a ply in x direction
j = jth segment of a space or a ply in y direction
k = kth segment of a ply in z'' direction
l = lth segment of a hole in z' direction
n = nth ply, space or hole
o = zero time
p = plugging time
S = DDS or SiC
T = $TiCl_4$ or TiB_2

Literature Cited

Besmann, T. M., and K. E. Spear, "Analysis of Chemical Vapor Deposition of Titanium Diboride: I. Equilibrium Thermodynamic Analysis," *J. Electrochem. Soc.: Solid-State Sci. and Tech.*, **124**(5), 786 (1977).

Besmann, T. M., and K. E. Spear, "Analysis of Chemical Vapor Deposition of Titanium Diboride: II. Modeling of Kinetics of Deposition," *J. Electrochem. Soc.: Solid-State Sci. and Tech.*, **124**(5), 790 (1977).

Bischoff, K. B., "Accuracy of the Pseudo Steady State Approximation for Moving Boundary Diffusion Problems," *Chem. Eng. Sci.*, **18**, 711 (1963).

Burganos, V. N., and S. V. Sotirchos, "Diffusion in Pore Networks: Effective Medium Theory and Smooth Field Approximation," *AIChE J.*, **33**(10), 1678 (1987).

Chung, G. Y., B. J. McCoy, J. M. Smith, D. E. Cagliostro, and M. Carswell, "Chemical Vapor Infiltration: Modelling Solid Matrix Deposition in Ceramic/Ceramic Composites," *Chem. Eng. Sci.*, **46**(3), 723 (1991).

Chung, G. Y., B. J. McCoy, J. M. Smith, and D. E. Cagliostro, "Chemical Vapor Infiltration: Modelling Solid Matrix Deposition for Ceramic Composites Reinforced with Layered Woven Fabrics," *Chem. Eng. Sci.*, **47**(2), 311 (1992).

Currier, R. P., "Overlap Model for Chemical Vapor Infiltration of Fibrous Yarns," *J. Amer. Ceram. Soc.*, **73**(8), 2274 (1990).

Froment, G. F., and K. B. Bischoff, *Chemical Reactor Analysis and Design*, Wiley, New York, p. 167 (1979).

Gupte, S. M., and J. A. Tsamopoulos, "Densification of Porous Material by Chemical Vapor Infiltration," *J. Electrochem. Soc.*, **136**(2), 555 (1989).

Gupte, S. M., and J. A., Tsamopoulos, "An Effective Medium Approach for Modelling Chemical Vapor Infiltration of Porous Ceramic Materials," *J. Electrochem. Soc.*, **137**(5), 1626 (1990).

Jensen, K. F., and R. R. Melkote, "Chemical Vapor Infiltration of Short Fiber Preforms," *Extended Abstract of AIChE Meeting*, San Francisco, p. 54 (1989).

Naslain, R., H. Hannache, L. Heraud, J. Y. Rossignol, F. Christin, and C. Bernard, "Chemical Vapor Infiltration Technique," *Proc. Europ. Conf. on Chemical Vapor Deposition*, p. 293 (1983).

Naslain, R., F. Langlais, and R. Fedou, "The CVI-Processing of Ceramic Matrix Composites," *J. de Phys. Coll. C5*, **50**(5), 191 (1989).

Peshev, P., and T. Niemyski, "Preparation of Crystalline Titanium Diboride by the Gas Phase Reaction," *J. Less-Common Metals*, **10**, 133 (1965).
Rossignol, J. Y., F. Langlais, and R. Naslain, "A Tenative Modelization of Titanium Carbide C.V.I. within the Pore Network of Two-Dimensional Carbon-Carbon Composite Preforms," *Proc. Electrochem. Soc.*, **84**(6), 596 (1984).
Smith, J. M., *Chemical Engineering Kinetics*, McGraw-Hill, New York, p. 414 (1970).
Sotirchos, S. V., and M. Tomadakis, "Modelling the Densification of Fibrous Structures," *Extended Abstract of AIChE Meeting*, San Francisco, p. 135 (1989).
Starr, T., "Model for CVI of Short Fiber Preforms," *Ceram. Eng. Sci. Proc.*, **8**(7), 951 (1987).
Tai, N. H., and T. W. Chou, "Analytical Modeling of Chemical Vapor Infiltration in Fabrication of Ceramic Composites," *J. Amer. Ceramic. Soc.*, **72**(3), 414 (1989).
van den Brekel, C. H. J., R. M. M. Fonville, P. J. M. van der Straten, and G. Verspui, "CVD of Ni, TiN, and TiC on Complex Shapes," *Proc. Electrochem. Soc.*, **81**, 142 (1981).
Wakao, N., and J. M. Smith, "Diffusion in Catalyst Pellets," *Chem. Eng. Sci.*, **17**, 825 (1962).

Manuscript received June 25, 1992, and revision received Mar. 10, 1993.